Generating nonclassical states from classical radiation by subtraction measurements

To cite this article: Luke C G Govia *et al* 2014 *New J. Phys.* **16** 045011

View the article online for updates and enhancements.

Generating nonclassical states from classical radiation by subtraction measurements

Luke C G Govia[1,2], **Emily J Pritchett**[1] **and Frank K Wilhelm**[1,2]

[1] Theoretical Physics, Universität des Saarlandes, Saarbrücken, Germany
[2] Institute for Quantum Computing and Department of Physics and Astronomy, University of Waterloo, ON, Canada
E-mail: s9lugovi@stud.uni-saarland.de

Abstract

We describe the creation of nonclassical states of microwave radiation via ideal dichotomic single photon detection, i.e., a detector that only indicates presence or absence of photons. Ideally, such a detector has a back action in the form of the subtraction operator (bare lowering operator). Using the non-linearity of this back action, it is possible to create a large family of nonclassical states of microwave radiation, including squeezed and multi-component cat states, starting from a coherent state. We discuss the applicability of this protocol to current experimental designs of Josephson photomultipliers.

Keywords: quantum computing, quantum information, superconducting circuits, microwave photonics

1. Introduction

The generation of nonclassical states of radiation is an important test of the foundations of quantum mechanics and a necessary precursor to implementing quantum communication and computation protocols in many architectures [1–3]. While the methodology for creating nonclassical radiation at optical wavelengths has been studied extensively [4–8], the technology to create quantum states with larger and larger wavelengths has recently become available with advances in cavity- and circuit-QED.

In this paper we present a novel way to generate a family of nonclassical states of microwave radiation in a long wavelength resonator using only detection by an ideal binary detector, such as the Josephson photomultiplier (JPM). The protocol only involves radiating a microwave cavity with coherent radiation and post selection based on single photon detection, without further manipulation. In addition, our protocol applies to any detection mechanism with a back action resembling that of the subtraction operator (equation (1)) and so can be generalized to other quantum systems, in particular, other superconducting circuits where strong photon-detector coupling is possible [9–11]. Recent proposals have established an analogous detection scheme in cavity-QED, broadening the range of application of our results [12, 13].

In the microwave regime of cavity-QED/circuit-QED squeezed states [14–16] and cat-like states [17, 18] of microwave radiation have been generated by the Kerr interaction between a cavity/transmission line and coupled atoms/superconducting qubits. Multi-component cat states have also been produced in circuit-QED using a gate-based construction [10, 11]. We show how these nonclassical states can be created in circuit-QED by a measurement based protocol, and add a new class of nonclassical states to the list, the generalized squeezed states, which so far have only been proposed in theory [19, 20].

The JPM, a current biased Josephson junction related to the phase qubit, has been shown experimentally [21] and theoretically [22–24] to be an effective single microwave photon counter. Previously, we have shown that for a JPM under optimal conditions (long relaxation time, short pure dephasing time, and a small dark count rate) the back action of photon detection is the photon subtraction operator [22],

$$\hat{B} \equiv \sum_{n=1}^{\infty} |n - 1\rangle\langle n|, \tag{1}$$

a nonlinear operator that can be related to the photon lowering operator by $\hat{a} = \hat{B}\sqrt{\hat{n}}$, but cannot be expressed as a linear combination of photon creation and annihilation operators. Also, note that $\hat{B}$ is not invertible, and hence not unitary. The JPM can be seen in this regime as an ideal dichotomic detector (see appendix A for further information), providing information about the presence or absence of photons but not revealing their number beyond that. Unlike traditional intensity meausurements, a measurement with subtraction operator back action has no corresponding classical observable, and as such has the potential to turn classical states into nonclassical ones.

2. Protocols for nonclassical state generation

In this paper we show how to use the noncommuntativity of the detection back action with coherent displacement pulses to achieve single mode quadrature squeezing of an input coherent state as well as to generate other nonclassical states, namely generalized squeezed states and squeezed multi-component Schrödinger cat states [4]. The subtraction operator is phase squeezing in particular as it removes the phases of the lower energy Fock states in the original coherent state superposition without changing the phases of the higher energy Fock states— which become the lower energy states—to compensate. Note that a special case of the second step of our protocol is already known in quantum optics: subtracting a photon from a squeezed vacuum state produces a low-power cat (kitten) state [7].

2.1. Squeezed states

The generation of squeezed states of microwave radiation using JPMs follows a simple protocol. The cavity is initially prepared in a coherent state, $|\alpha\rangle = \hat{D}(\alpha)|0\rangle = e^{-\frac{|\alpha|^2}{2}} \sum_{n=0}^{\infty} \frac{\alpha^n}{\sqrt{n!}} |n\rangle$ where $\alpha \equiv |\alpha| e^{i\varphi_\alpha}$, and is coupled to one or more detectors, each acting with back action $\hat{B}$ on the cavity after a photon is detected. Mathematically a coherent displacement such as this is represented by the displacement operator $\hat{D}(\alpha) = e^{(\alpha \hat{a}^\dagger - \alpha^* \hat{a})}$. After N photons are counted (either by N detectors, or less if fast detector reset is possible), a further displacement pulse is applied such that the state is centred around $-\alpha$ in phase space. After N further photon detections are observed, the resulting state is a squeezed state. The optimal choice of N will be discussed shortly.

Starting from the coherent state input, the probability for N photons to be detected is

$$P_N \equiv 1 - e^{-|\alpha|^2} \sum_{n=0}^{N-1} \frac{|\alpha|^{2n}}{n!} = 1 - \frac{\Gamma(N, |\alpha|^2)}{\Gamma(N)} \tag{2}$$

where $\Gamma(N, |\alpha|^2)$ is the upper incomplete gamma function of N and $|\alpha|^2$ [25]. $P_N \sim |\alpha|^{2N}/N!$ as $|\alpha| \to 0$; however, at $|\alpha|^2 \approx N$ P_N jumps rapidly towards unity, and so can be made arbitrarily close to unity with higher power coherent pulses (see appendix C for further details).

It is straightforward to calculate the normalized post measurement cavity state after N detections,

$$\rho' \equiv \frac{\hat{B}^N |\alpha\rangle \langle \alpha| \hat{B}^{\dagger N}}{P_N}, \tag{3}$$

and the average photon number $n_1 \equiv \langle a^\dagger a \rangle_{\rho'}$ is given by

$$n_1 = \frac{|\alpha|^2 \left(1 - \frac{\Gamma(N-1, |\alpha|^2)}{\Gamma(N-1)}\right) - N \left(1 - \frac{\Gamma(N, |\alpha|^2)}{\Gamma(N)}\right)}{P_N}, \tag{4}$$

which can also be numerically evaluated. After N detections, the next step is to displace the state by an amount $\alpha_1 = -\sqrt{n_1} e^{i\varphi_\alpha} - \alpha$, so that the resulting state will be centred in phase space around $-\alpha$. For this displaced state, N photon detection events will occur with probability P_N' [3], and the renormalized cavity state will have the form

$$\rho'' \equiv \frac{\hat{B}^N D(\alpha') \rho' D(\alpha')^\dagger \hat{B}^{\dagger N}}{P_N'}. \tag{5}$$

We will now show that the state ρ'' is a squeezed state.

To quantify the amount of squeezing, we calculate the variance of the squeezed quadrature

$$\Delta p^2 = \text{Tr}\left[\rho'' \hat{p}^2\right] - \text{Tr}\left[\rho'' \hat{p}\right]^2. \tag{6}$$

The quadrature observable $\hat{p}(\varphi_\alpha)$ is defined by $\hat{p}(\varphi_\alpha) = \frac{i}{\sqrt{2}}(\hat{a}^\dagger e^{i\varphi_\alpha} - \hat{a} e^{-i\varphi_\alpha})$, where $\hat{a}$ is the annihilation operator for the cavity microwave mode. The phase shift $e^{-i\varphi_\alpha}$ accounts for the fact

---

[3] For which the analytic expression is cumbersome and not instructive but, as is the case for P_N, $P_N' \to 1$ for $|\alpha| \to \infty$.

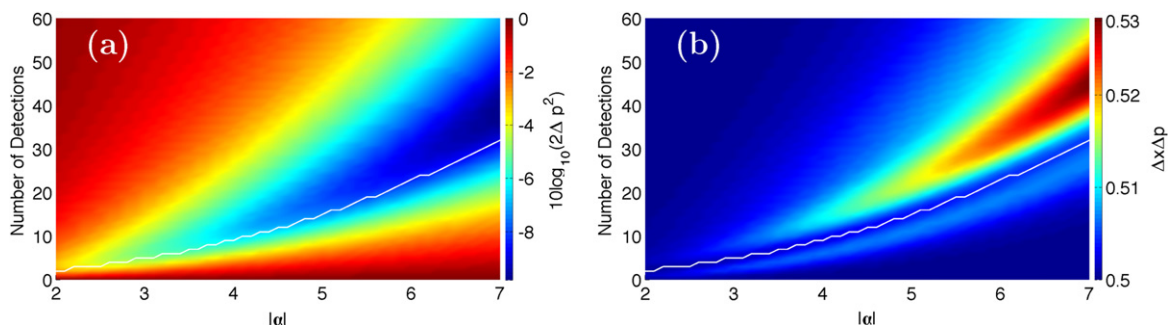**Figure 1.** (a) $S(\Delta p)$ and (b) $\Delta x \Delta p$ of the state ρ'', as functions of α and the number of detection events, N. $\varphi_\alpha = 0$ for both figures. The white curve indicates the value of N that gives a local minimum in $\Delta x \Delta p$, while maintaining a squeezed Δp^2.

that this protocol squeezes along the phase space axis complementary to that defined by the phase of the input coherent state. Anything less than $\Delta p^2 = \frac{1}{2}$ indicates a squeezed state. The amount of squeezing is expressed in dB, by calculating

$$S(\Delta p) \equiv 10 \log_{10} \left(\frac{\Delta p^2}{\Delta p^2_{\text{norm}}} \right) = 10 \log_{10} (2\Delta p^2). \tag{7}$$

In addition, we can calculate how far the state ρ'' deviates form a minimal uncertainty state by calculating $\Delta x \Delta p$ (where $\hat{x} = \frac{1}{\sqrt{2}} (\hat{a} e^{-i\varphi_\alpha} + \hat{a}^\dagger e^{i\varphi_\alpha})$ is the conjugate observable to $\hat{p}$). Figures 1(a) and (b) show $S(\Delta p)$ and $\Delta x \Delta p$ respectively as functions of α and the number of detection events on either side of the displacement, N.

As can be see in figure 1(a), the maximum amount of squeezing possible on a given input state $|\alpha\rangle$ increases monotonically with $|\alpha|^2$, proportional to the power of the input pulse. Interestingly, for a given α, there exists a finite N that achieves a global minimum in Δp^2. One would be tempted to use this value of N in the protocol to create ρ''; however, as can be seen in figure 1(b), there are other concerns.

As figure 1(b) shows, for a given α, $\Delta x \Delta p$ is not monotonic in N. Since we want ρ'' to be as close to a minimal uncertainty state as possible, while still maintaining a significantly squeezed quadrature, the optimal choice of N for the protocol would be at the $\Delta x \Delta p$ local minima shown in figures 1(a) and (b) by the white curve. While this does not minimize Δp^2 (and therefore maximize squeezing), it achieves a significantly squeezed state ρ'' that is as close to being a minimal uncertainty state as is possible, which is what we consider optimal.

2.2. Generalized squeezed states

Other nonclassical states of microwave radiation having $\varphi_k \equiv 2\pi/k$ rotational symmetry in phase space result from generalizing this procedure (see figure 2). The squeezed state protocol discussed previously involves detecting the cavity state while centred at two points on a line through the origin of phase space, i.e. the case $k = 2$. To generalize this protocol, we detect N photons at k positions equally spaced around a circle of radius $|\alpha|$ in phase space, and take the first position on the positive real axis for simplicity.
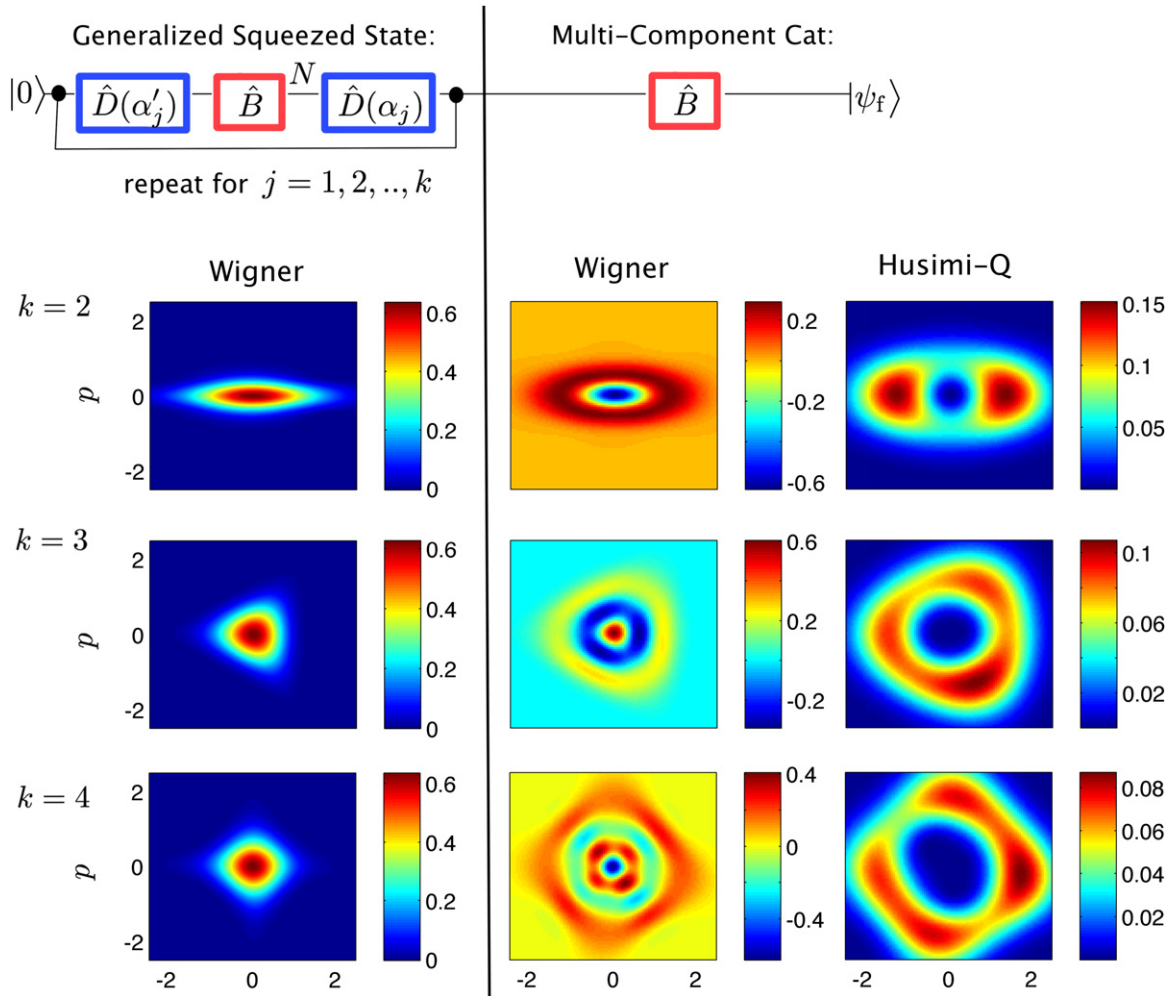
Figure 2. (upper) A schematic description of the state preparation protocol. (lower) Wigner representations (first and second columns) and Husmi Q representations (third column) of the $k = 2$, $k = 3$, and $k = 4$ generalized squeezed vacuum states (first column) and squeezed k-component Schrödinger cat states (second and third columns). The Wigner functions have been scaled such that they correspond to the quadrature opertors defined previously scaled by a factor of $1/\sqrt{2}$. Note that the second column has non-uniform colour bars for its figures in order to highlight all relevant information. Appendix D contains a table of the fidelities, success probabilities, and α, δ, and N values for these states, as well as the fit parameters z and β.

There are k steps to this generalized protocol, and for $j = 0, 1, ..k - 1$, the jth step is to: (1) displace by α_j so that the cavity state is centred around $|\alpha| e^{ij\varphi_k}$, (2) detect N photons, and (3) displace by α'_j, such that the cavity state is centred around the origin, where the coherent displacements parameters are

$$\alpha_j = |\alpha| e^{ij\varphi_k} \tag{8}$$

$$\alpha'_j = -\delta_j e^{ij\varphi_k} \tag{9}$$

$$\delta_j \approx \sqrt{n_j}. \tag{10}$$

The amplitude of the displacement to the origin, δ_j, is approximately the square root of the photon number left in the cavity after N detections, with a small correction accounting for the asymmetry of the intermediate states of the protocol.

Finally, after detecting N photons at all k positions, we obtain the generalized squeezed state with k-fold symmetry, ρ_k. The detection stage at each position transforms ρ_{j1} to ρ_{j2} according to

$$\rho_{j2} \equiv \frac{\hat{B}^N \rho_{j1} \hat{B}^{\dagger N}}{P_N^j}, \tag{11}$$

where P_N^j is the probability of detecting N photons from the state ρ_{j1}. The entire protocol will complete with success probability

$$\mathrm{Prob}(\mathrm{success}) = \prod_{j=0}^{k-1} P_N^j, \tag{12}$$

which can be made close to unity (see appendix C).

As mentioned previously, the case $k = 2$ ($\varphi_k = \pi$) corresponds to the creation of the vacuum with squeezed quadratures. We find high (here and henceforth meaning above 99%) overlap with

$$|\Psi_2\rangle = S(z)|0\rangle = e^{-\frac{1}{2}(z(\hat{a}^\dagger)^2 - z^*(\hat{a})^2)} |0\rangle \tag{13}$$

by numerically searching over N and z, where $S(z)$ is the ordinary squeezing operator with complex squeezing parameter z. In general, for $k \geqslant 2$, the states created by this protocol have high overlap with the analytic states

$$|\Psi_k\rangle = S^{(k)}(z)|0\rangle = e^{-\frac{1}{2}(z(\hat{a}^\dagger)^2 - z^*(\hat{a})^2)}|0\rangle, \tag{14}$$

where $S^{(k)}(z)$ is called a generalized squeezing operator with complex parameter z [19, 20]. The first three operators of this class are

$$S^{(0)}(z) = e^{-\mathrm{Im}[z]}\mathbb{1}, \; S^{(1)}(z) = D\left(-\frac{z}{2}\right) \text{and} \;\; S^{(2)}(z) = S(z), \tag{15}$$

where $S(z)$ is the squeezing operator of equation (13).

Consider the final state after displacing to the origin ρ_k. To find z, we impose the condition that ρ_k and $|\Psi_k\rangle$ have the same average photon number by setting

$$\langle\Psi_k|\hat{a}^\dagger\hat{a}|\Psi_k\rangle = \langle\hat{a}^\dagger\hat{a}\rangle_{\rho_k}. \tag{16}$$

This results in excellent fidelity between the states, quantified by

$$F[\rho_k] \equiv \mathrm{Tr}\left\{\rho_k \; |\Psi_k\rangle\langle\Psi_k|\right\}. \tag{17}$$

In fact, for $k = 2, 3, 4$ the fidelity is greater than 99% in each case for various values of $|\alpha|$. The Wigner functions of these states are shown in the left column of figure 2.

To verify that these states are indeed nonclassical, a suitable nonclassicality witness can be used. For this purpose, we use the entanglement potential of [26], where a nonzero entanglement potential indicates that a state is nonclassical. Indeed, as can be calculated numerically, the states created by the generalized protocol all have nonzero entanglement potential (see appendix B).

Since the first displacement stage of each step ensures the average photon number of each state ρ_{j1} is on the order of $|\alpha|^2$, each P_N^j can be quite large, and as a result, the generalized protocol can have a significant probability of success. For example, for the modest $|\alpha|$ of the states shown in figure 2, the success probabilities are all greater than 99%. Furthermore, the success probability will grow monotonically with $|\alpha|$, and so can be increased by increasing the initial input state power.

2.3. Squeezed multi-component cat states

It is known in quantum optics [7] that subtracting a photon from a squeezed vacuum produces an odd Schrödinger cat state. This concept can be generalized, such that subtracting a photon from a generalized squeezed vacuum of k-fold symmetry (the output state ρ_k of our protocol in 2.2) leaves a squeezed, k-component Schrödinger cat state in the cavity. We note that while having some similarity to the optical setting, our protocol does not require a beam splitter or a photon number resolving detector, instead, it simply requires the subtraction of one more photon from the squeezed states created by the protocol described in the previous section.

If we remove one more photon from the final state ρ_k, the resulting state has the form

$$\rho_k' = \frac{\hat{B}\rho_k\hat{B}^\dagger}{P_1^k},\tag{18}$$

where P_1^k is the probability of a single photon being detected from state ρ_k. This procedure produces states of high overlap with

$$\left|\Psi_k'\right\rangle = S^{(k)}(z)\sum_{j=0}^{k-1} e^{ij(\varphi_k+\pi)}\left|\beta e^{ij\left(\varphi_k+\pi\right)}\right\rangle,\tag{19}$$

where now both $z \in \mathbb{C}$ and $\beta \in \mathbb{R}$ must be found numerically. These states all have non-zero entanglement potential, and are therefore nonclassical states of microwave radiation (see appendix B).

For $k = 2$, this additional detection will create a state very close to a squeezed odd Schrödinger cat state

$$|\Psi_2'\rangle = S^{(2)}(z)(|\beta\rangle - |-\beta\rangle).\tag{20}$$

For $k = 3$ and $k = 4$, we have

$$|\Psi_3'\rangle = S^{(3)}(z)(e^{-i\frac{\pi}{3}}|\beta e^{-i\frac{\pi}{3}}\rangle + e^{i\frac{\pi}{3}}|\beta e^{i\frac{\pi}{3}}\rangle - |-\beta\rangle)\tag{21}$$

$$|\Psi_4'\rangle = S^{(4)}(z)(|\beta\rangle + i|i\beta\rangle - |-\beta\rangle - i|-i\beta\rangle).\tag{22}$$

The $k = 3$ state is the state formed when the operator $S^{(3)}(z)$ is applied to a voodoo cat state [11]. The $k = 4$ state is the operator $S^{(4)}(z)$ applied to a coherent superposition of four out of phase coherent states, known as a compass state, which is known to have favourable decoherence

properties [17, 27]. The Wigner and Husimi Q functions of these squeezed multi-component cat states are shown in the middle and right columns of figure 2 respectively, all of which have greater than 94% fidelity with (20), (21) and (22).

We have plotted both representations of these states as they highlight distinct information about the state. The Q function emphasizes the cat-like properties of the final state, while the Wigner function makes apparent the similarity between the final state and a $k - 1$ photon Fock state, squeezed to the same order in k. The highly nonclassical nature of the state is also made evident by the large negative region of its Wigner function.

The probability of successful generation of these multi-component cat states is

$$\text{Prob}(\text{success})' = P_1^k \prod_{j=0}^{k-1} P_N^j. \tag{23}$$

Unfortunately, the P_1^k are often very small, and for the squeezed multi-component cat states shown in figure 2 this results in a much lower success probability than the generalized squeezed vacuum. Optimization of this success probability is discussed in appendices C and D.

3. Discussion

3.1. Experimental implementation

In regards to experimental implementation of this protocol with JPMs, superconducting microwave resonators are currently fabricated with Q-factors approaching 10^7, which in the microwave regime will lead to cavity lifetimes on the order of 10^5 ns [28]. Thus, when JPMs with short T_2 are used [22], we can conservatively expect that as many as 10^2 to 10^3 measurements can be performed in the lifetime of the cavity. Practically, space requirements on a chip require a fast reset strategy for the JPMs, which is currently being developed [29].

For a realistic implementation of this protocol via JPMs, one must also consider the possibility of energy dissipation and dark counts in the JPMs. The behaviour of a JPM under such conditions has previously been discussed in [22, 23], and as such, we will highlight only the key point here. Both energy relaxation in the detector, and dark counts can be treated on the same footing. Energy relaxation corresponds to an unregistered measurement, and dark counts to false positives. One can thus adjust the number of measurements according to these rates to approach the desired number of $\hat{B}$-applications.

In the presence of dark counts and energy relaxation, one must describe the state of the cavity by a classically mixed state, with mixture components corresponding to different photon numbers in the cavity. However, in line with the standard interpretation of quantum mechanics, this mixing is only a lack of complete information on the observer's part, not on the action of the JPM. During each step of the protocol a definite number of photons is removed from the cavity, leaving it in a pure state. While we may be unaware of this exact number, unless this number plays a significant role in the success and performance of our protocol, or to further applications of the states created, then the mixture components are practically indistinguishable.

To that effect, as is illustrated in figure 1(a), the asymmetric squeezing performed at the j'th step is a smooth and slowly varying function of N, and as such is only minimally affected by a small change in N. Thus, the protocol is generally robust to the effects of energy relaxation and dark counts, provided these effects are small. Only the final detection used to generate

squeezed multi-component cat states is sensitive to small perturbations in N, with an odd number of detections producing states of the form seen in equation (19).

Photon lifetimes are in general a limiting factor for nonclassical states, but these have been reported to be very long in circuit QED (on the order of 100 μs in [17]), and given the fast measurement times of our protocol, the cavity lifetime will affect our protocol less than others. In addition, some of the nonclassical states created by our protocol are robust to photon loss. For example, the even k-th order squeezed states are robust to single photon loss [30].

3.2. Applications

The generalized squeezed states have applications in continuous variable quantum computing [31]. Our protocol provides a simple way to obtain the necessary single mode squeezing and nonlinearity: by applying the generalized squeezed state protocols for $k = 2$ and $k \geqslant 3$ respectively. In particular, implementing the nonlinearity is often the technological bottleneck, as it cannot be created using linear optics alone [32], and our proposal is to use the nonlinear transformation performed by our protocol for $k \geqslant 3$ in place of traditional nonlinear interactions (such as Kerr-like interactions). In this regard, our protocol has the potential to be more efficient and require less technological overhead than most known methods to implement the nonlinearity [32, 33].

The squeezed multi-component Schrödinger cat states (SMCS) have applications in metrology, in particular for phase estimation using a Mach–Zehnder interferometer set up. It has recently been shown that cat states can be used in combination with linear optics to create entangled coherent states (ECS), and that phase estimation using these ECS outperforms that using NOON states [34]. The performance difference is especially significant at low photon number, and/or when photon loss is considered. It is an emerging and active area of research to see if an improvement in phase estimation can be gained by using SMCS in place of cat states in this scheme.

3.3. Conclusions

In conclusion, we have shown how a combination of strongly coupled photon counting and coherent displacement can be used to create nonclassical states of radiation with high probability (greater than 99% for the generalized squeezed states), and with high fidelity (greater than 99% for the generalized squeezed states, and greater than 94% for the squeezed multi-component cats). This protocol can be realized in circuit QED using JPM.

Appendix A. The JPM

The JPM consists of a current biased Josephson junction which can be completely described by the phase difference across the junction, and its conjugate momentum (related to the charge

difference across the junction). Such a system has a potential energy (as a function of phase) which has the so called 'tilted washboard' shape:

$$U(\phi) \approx -I_c \cos\phi - I_b\phi \qquad (A.1)$$

where I_c is the junction critical current and I_b is the applied bias current.

The system thus has an infinite number of local energy minima which have one or more metastable bound states. The applied bias current determines the number of bound states, and during operation the JPM is biased such that the potential minimum working point contains only two metastable bound states. Additionally, during operation, the bias current is finely tuned such that the energy difference between the metastable bound states is equal to the photon energy of the microwave cavity coupled to the JPM. It is important to note that the control offered by the applied bias makes the JPM tunable, allowing one to bring it in and out of strong coupling with the microwave cavity.

The detection mechanism of the JPM relies on the fact that the bound states of the potential well are metastable, and have finite quantum tunnelling rates out of the potential well. These rates increase exponentially as the excitation number in the potential well increases. When there are only two metastable states in the potential well, tunnelling out of the ground state is exponentially suppressed, and all observed tunnelling events can be attributed to incident microwave radiation exciting the JPM into the excited metastable state, and this state then tunnelling out of the potential well. A tunnelling event results in a large voltage change across the circuit, and as a result can be detected by external classical circuitry. We can thus equate a tunnelling event with a single photon detection.

In reference [22] the back action of the JPM onto the microwave cavity was thoroughly examined, taking into account the relevant physical processes occurring (JPM relaxation and pure dephasing, and tunnelling out of the metastable ground state). We will briefly summarize the points relevant to this work.

Photon detection by a JPM approaches the dichotomic detection of the subtraction operator when the JPM and the cavity are allowed to interact for a long enough time (typically several Rabi periods) before the tunnelling event occurs. This is achieved when the coupling strength between the JPM and the cavity is comparable to the tunnel rate out of the first excited metastable state, as achieved in [21]. This 'long' interaction time removes any photon number information in the measurement time coming from the $\sqrt{n}\,g$ dependent oscillation periods of the Fock states.

However, the long interaction time with the JPM results in the reduction of the coherence between cavity Fock states after measurement, something that is not caused by the subtraction operator. To counteract this affect, a JPM with a short T_2 time can be used, since pure dephasing effectively kills the cavity coherence damping effect of the JPM (see [22], figure 3(b)). In the extreme case where the cavity–JPM interaction is itself incoherent, the subtraction operator back action is obtained.

Appendix B. Nonclassicality

The entanglement potential is both a nonclassicality witness and measure, and as such can be used to examine how the nonclassicality changes with the number of detections at each step of the generalized protocol. It is defined as

$$EP[\rho] \equiv \log_2 \|\sigma_\rho^{T_A}\|_1,\tag{B.1}$$

where $\sigma_\rho = U_{BS}(\rho \otimes |0\rangle\langle 0|)U_{BS}^\dagger$, for U_{BS} the unitary transformation of a 50:50 beam splitter, and $\sigma_\rho^{T_A}$ is the partial transpose of σ_ρ [35]. Figure B1 shows the entanglement potential of the generalized squeezed states and the multi-component cat states (for $k = 2, 3, 4$) as a function of the number of detections at each step. As can be seen, for the squeezed state ($k = 2$), the maximum value of EP occurs around the optimal value of N determined in the main text.

Appendix C. Success probability versus fidelity

Due to the noncommutivity of the subtraction operator and coherent displacement, finding a simple closed form analytic solution for the success probability of our protocols (equations (12) and (23)) may not be possible. However, we can examine the behaviour of P_N of equation (2) to understand how the total detection probability scales with $|\alpha|^2$. As can be seen in figure C1(a), P_N rapidly approaches unity for $|\alpha|^2 > N$. As a result of this, it is possible to achieve very high success probabilities for the generalized squeezed state protocol. For the squeezed multi-component cat states, the limiting factor remains P_1^k, which can be quite small.

In addition to success probability, one also wishes to maximize the fidelity with the target analytic states. In the $k = 2$ case, we find that this is achieved when, for a given $|\alpha|$, N lies nearly along the minimal uncertainty curve of figure 1(b). This curve is well approximated by $q(|\alpha|) = a|\alpha|^2 + b|\alpha| + c$, where $a, b, c \in \mathbb{R}$ can be found numerically. Since N must be an integer, we set

$$N = \lceil q(|\alpha|) \rceil,\tag{C.1}$$

where $\lceil * \rceil$ rounds up to the nearest integer. It is worth examining what effect this has on the success probability of P_N, now defined by

$$P_N = 1 - \frac{\Gamma(\lceil q(|\alpha|) \rceil, |\alpha|^2)}{\Gamma(\lceil q(|\alpha|) \rceil)}.\tag{C.2}$$

This is plotted in figure C1(b), along with the continuous version of equation (C.2), where N is allowed to take non-integer values. As the figures show, the success probability approaches unity with increasing $|\alpha|$. It is therefore possible to maximize both fidelity and success probability in the $k = 2$ case, for both the squeezed state and Schrödinger cat state.

For $k > 2$ there is no known analog of the minimal uncertainty curve of figure 1(b), however, numerical results have shown that it is possible to achieve high fidelity and success probability using N and $|\alpha|$ similar to that of the $k = 2$ case, i.e. near to the minimal uncertainty curve.

Appendix D. Numerical results

In figure 2, we have given examples of a generalized squeezed vacuum and a squeezed/multi-component cat, for $k = 2, 3, 4$. Each of these examples is found by a numerical fit over the parameters in the protocol: the field amplitude α, the number of photon subtractions at each position N, and the small corrections for photon loss, $\delta_1, .., \delta_k$. For each of the examples in
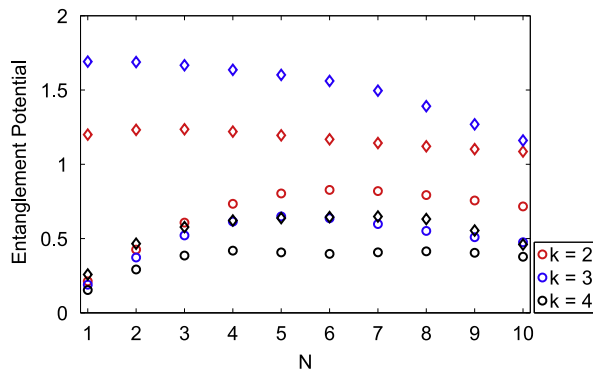
Figure B1. This figure shows entanglement potential (EP) of the states created by the generalized protocol (for $k = 2, 3, 4$) as a function of the number of detections, N, performed at each step in the protocol. The generalized squeezed states are the circles, and the diamonds correspond to the squeezed multi-component cat states. These states all have $|\alpha| = 3$.
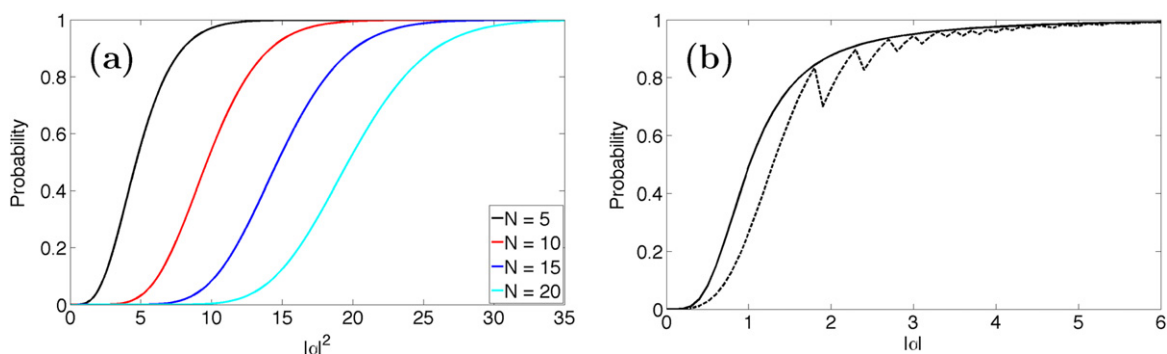

Figure C1. The success probability of the first step of the protocol as a function of input coherent state power. In (a) for several values of fixed N, and in (b) for N assumed to vary quadratically as $q(|\alpha|)$. The solid line in (b) is for N taking real values, and the dashed line for N taking only integer values.

figure 2, we have locally minimized the error function

$$\epsilon = 1 - F[\rho_k, \rho_k^{\mathrm{t}}] \tag{D.1}$$

over the set of parameters $\mathcal{P} = \{x_i\}$ necessary to define ρ_k—the final state produced in our protocol—and the target state $\rho_k^{\mathrm{t}} = |\Psi_k\rangle\langle\Psi_k|$. The fidelity F is as defined in equation (17). We have given examples only for $N = 16$ ($N = 6$ in the case of the 4-component cat state) to reduce this parameter space. Although this choice is somewhat arbitrary, it generally predicts reasonably small error for $|\alpha| \in [3, 10]$, an experimentally accessible range.

In the case of the generalized squeezed vacuum states, we constrain the squeezing parameter z, all that is necessary to specify the target state, so that

$$\langle \hat{n} \rangle_{\rho_k} = \langle \hat{n} \rangle_{\rho_k^{\mathrm{t}}}. \tag{D.2}$$

		generalized squeezed vacuums		
k=2	$\alpha = 5.7389$			
	$\delta_1 = 1.6786$	$\delta_2 = 1.7227$		
	$z = 0.7063$			
	$P = 0.9951$	$\epsilon^{(2)} = 1.7 \times 10^{-3}$		
k=3	$\alpha = 6.6999$			
	$\delta_1 = 1.1782$	$\delta_2 = 1.1536$	$\delta_3 = 1.1532$	
	$z = -0.185$			
	$P = 1.0000$	$\epsilon^{(3)} = 4.5 \times 10^{-4}$		
k=4	$\alpha = 5.9999$			
	$\delta_1 = 1.2138$	$\delta_2 = 1.2166$	$\delta_3 = 1.2047$	$\delta_4 = 1.2193$
	$z = 1.4776$			
	$P = 0.9999$	$\epsilon^{(4)} = 6.1 \times 10^{-3}$		
		squeezed multi-component cats		
k=2	$\alpha = 3.8480$			
	$\delta_1 = 1.9783$	$\delta_2 = 1.5670$		
	$z = -3.8667$	$\beta = 2.00$		
	$P = 0.2478$	$\epsilon^{(2)} = 2.0 \times 10^{-3}$		
k=3	$\alpha = 7.5000$			
	$\delta_1 = 1.582$	$\delta_2 = 1.1522$	$\delta_3 = 1.1482$	
	$z = 4.4 \times 10^{-2}$	$\beta = 6.0 \times 10^{-5}$		
	$P = 0.0037$	$\epsilon^{(3)} = 4.4 \times 10^{-3}$		
k=4	$\alpha = 3.5500$			
	$\delta_1 = 0.9451$	$\delta_2 = 0.9518$	$\delta_3 = 0.9393$	$\delta_4 = 0.9401$
	$z = 0.0014$	$\beta = 1.56$		
	$P = 0.0025$	$\epsilon^{(4)} = 5.6 \times 10^{-2}$		

Figure D1. Protocol parameters α and $\{\delta_j\}$, target state parameter(s) z (and β), error ϵ^k, and corresponding success probability P for each of the examples given in figure 2. $N = 16$ in all cases except for the 4-component cat, in which case $N = 6$.

There remains $k + 1$ unconstrained parameters determining the error function:

$$\epsilon^k \equiv \epsilon^k(\alpha, \delta_1, .., \delta_k). \tag{D.3}$$

In the case of multi-component/squeezed cats, two parameters specify ρ_k^{t}, z and the cat-state amplitude β. In this case, β is constrained according to equation (D.2), and we add z to the set of parameters over which we minimize the error:

$$\epsilon^k \equiv \epsilon^k(z, \alpha, \delta_1, .., \delta_k). \tag{D.4}$$

Figure D1 contains the parameter values, ϵ^k, and success probabilities P for each of the cases shown in figure 2.

Note that the error function equation (D.1) is multimodal, so we have not likely found a global maximum in state fidelity. Generally, the detection probability is also multimodal when the integer nature of N is considered, e.g. see dotted curve in figure C1(b), so the detection probabilities listed here are not likely maximal and depend sensitively on the choice of N. While our choice $N = 16$ is well-suited for $k = 2$, other values would likely optimize the cat-state detection probabilities for different k. We leave the optimal value of N for a given k as an open question.

References

[1] Knill E, Laflamme R and Milburn G J 2001 A scheme for efficient quantum computing with linear optics *Nature* **409** 46

[2] Braunstein S L and van Loock P 2005 Quantum information with continuous variables *Rev. Mod. Phys.* **77** 513

[3] Gisin N, Ribordy R, Tittel W and Zbinden H 2002 Quantum cryptography *Rev. Mod. Phys.* **74** 145

[4] Lvovsky A I and Raymer M G 2009 Continuous-variable optical quantum-state tomography *Rev. Mod. Phys.* **81** 299–332

[5] Ourjoumtsev A, Tualle-Brouri R, Laurat J and Grangier P 2006 Generating optical Schrödinger kittens for quantum information processing *Science* **312** 83–86

[6] Shi-Biao Z 2005 Preparation of multicomponent Schrödinger cat states through resonant atom-field interaction *Commun. Theor. Phys.* **43** 1105

[7] Dakna M, Anhut T, Opatrný T, Knöll L and Welsch D-G 1997 Generating Schrödinger-cat-like states by means of conditional measurements on a beam splitter *Phys. Rev.* A **55** 3184–94

[8] Fiurášek J, García-Patrón R and Cerf N J 2005 Conditional generation of arbitrary single-mode quantum states of light by repeated photon subtractions *Phys. Rev.* A **72** 033822

[9] Akhlaghi M K, Majedi A H and Lundeen J S 2011 Nonlinearity in single photon detection: modeling and quantum tomography *Opt. Express* **19** 21305–12

[10] Hofheinz M, Weig E M, Ansmann M, Bialczak R C, Lucero E, Neeley M, O'Connell A D, Wang H, Martinis J M and Cleland A N 2008 Generation of Fock states in a superconducting quantum circuit *Nature* **454** 310–4

[11] Hofheinz M *et al* 2009 Synthesizing arbitrary quantum states in a superconducting resonator *Nature* **459** 546–9

[12] Raimond J M, Sayrin C, Gleyzes S, Dotsenko I, Brune M, Haroche S, Facchi P and Pascazio S 2010 Phase space tweezers for tailoring cavity fields by quantum Zeno dynamics *Phys. Rev. Lett.* **105** 213601

[13] Daniel K L O, Potoček V and Jeffers J 2013 Nondemolition measurement of the vacuum state or its complement *Phys. Rev. Lett.* **110** 210504

[14] Castellanos-Beltran M A, Irwin K D, Hilton G C, Vale L R and Lehnert K W 2008 Amplification and squeezing of quantum noise with a tunable Josephson metamaterial *Nat. Phys.* **4** 929–31

[15] Eichler C, Bozyigit D, Lang C, Baur M, Steffen L, Fink J M, Filipp S and Wallraff A 2011 Observation of two-mode squeezing in the microwave frequency domain *Phys. Rev. Lett.* **107** 113601

[16] Wilson C M, Johannsson G, Pourkabirian A, Johannson J R, Duty T, Nori F and Delsing P 2011 Observation of the dynamical Casimir effect in a superconducting circuit *Nature* **479** 376

[17] Kirchmair G, Vlastakis B, Leghtas Z, Nigg S E, Paik H, Ginossar E, Mirrahimi M, Frunzio L, Girvin S M and Schoelkopf R J 2013 Observation of quantum state collapse and revival due to the single-photon Kerr effect *Nature* **495** 205–9

[18] Deleglise S, Dotsenko I, Sayrin C, Bernu J, Brune M, Raimond J-M and Haroche S 2008 Reconstruction of non-classical cavity field states with snapshots of their decoherence *Nature* **455** 510–4

[19] Braunstein S L and McLachlan R I 1987 Generalized squeezing *Phys. Rev.* A **35** 1659–67

[20] Braunstein S L and Caves C M 1990 Phase and homodyne statistics of generalized squeezed states *Phys. Rev.* A **42** 4115–9

[21] Chen Y-F, Hover D, Sendelbach S, Maurer L, Merkel S T, Pritchett E J, Wilhelm F K and McDermott R 2011 Microwave photon counter based on Josephson junctions *Phys. Rev. Lett.* **107** 217401

[22] Govia L C G, Pritchett E J, Merkel S T, Pineau D and Wilhelm F K 2012 Theory of Josephson photomultipliers: optimal working conditions and back action *Phys. Rev.* A **86** 032311

[23] Poudel A, McDermott R and Vavilov M G 2012 Quantum efficiency of a microwave photon detector based on a current-biased Josephson junction *Phys. Rev.* B **86** 174506

[24] Peropadre B, Romero G, Johansson G, Wilson C M, Solano E and Garcia-Ripoll J J 2011 Approaching perfect microwave photodetection in circuit QED *Phys. Rev.* A **84** 063834

[25] Arfken G B, Weber H J and Harris F E 2012 *Mathematical Methods for Physicists: A Comprehensive Guide* 7th edn (Waltham, MA: Academic Press)

[26] Asbóth J K, Calsamiglia J and Ritsch H 2005 Computable measure of nonclassicality for light *Phys. Rev. Lett.* **94** 173602

[27] Zurek W H 2001 Sub-Planck structure in phase space and its relevance for quantum decoherence *Nature* **412** 712–7

[28] Megrant A *et al* 2012 Planar superconducting resonators with internal quality factors above one million *Appl. Phys. Lett.* **100** 113510

[29] McDermott R 2012 private communication

[30] Leghtas Z, Kirchmair G, Vlastakis B, Schoelkopf R J, Devoret M H and Mirrahimi M 2013 Hardware-efficient autonomous quantum memory protection *Phys. Rev. Lett.* **111** 120501

[31] Lloyd S and Braunstein S L 1999 Quantum computation over continuous variables *Phys. Rev. Lett.* **82** 1784–7

[32] Bartlett S D and Sanders B C 2002 Universal continuous-variable quantum computation: requirement of optical nonlinearity for photon counting *Phys. Rev.* A **65** 042304

[33] Milburn G J and Walls D F 1983 Quantum nondemolition measurements via quadratic coupling *Phys. Rev.* A **28** 2065–70

[34] Joo J, Munro W J and Spiller T P 2011 Quantum metrology with entangled coherent states *Phys. Rev. Lett.* **107** 083601

[35] Vidal G and Werner R F 2002 Computable measure of entanglement *Phys. Rev.* A **65** 032314